Spatial decomposition of magnetic anisotropy in magnets: Application to doped $Fe_{16}N_2$

Yang Sun,[1] Yong-Xin Yao,[2] Manh Cuong Nguyen,[2,*] Cai-Zhuang Wang,[2] Kai-Ming Ho,[2] and Vladimir Antropov[2,†]
[1]*Department of Applied Physics and Applied Mathematics, Columbia University, New York, New York 10027, USA*
[2]*Ames Laboratory, US DOE and Department of Physics, Iowa State University, Ames, Iowa 50011, USA*

(Received 22 June 2020; revised 9 September 2020; accepted 7 October 2020; published 22 October 2020)

We propose a scheme of decomposition of the total relativistic energy in solids to intra- and interatomic contributions. The method is based on a site variation of such fundamental constant as the speed of light. As a practical illustration of the method, we tested such decomposition in the case of a spin-orbit interaction variation for the decomposition of the magnetic anisotropy energy (MAE) in CoPt. We further studied the α''-$Fe_{16}N_2$ magnet doped by Bi, Sb, Co, and Pt atoms. It was found that the addition of Pt atoms can enhance the MAE by as much as five times while Bi and Sb substitutions double the total MAE. Using the proposed technique, we demonstrate the spatial distribution of these enhancements. Our studies also suggest that Sb, Pt, and Co substitutions could be synthesized by experiments.

DOI: 10.1103/PhysRevB.102.134429

I. INTRODUCTION

Today, studies of magnetic anisotropy (MA) are very popular due to many existing and potential applications of certain magnets as well as a very rich microscopic physics of these materials. The strength of MA effects is usually relatively small, and because of this they have been called for years "secondary" magnetic effects. Initial MA models [1–3] employed very simplified ideas of "single-ion" anisotropy and could not be applied for metallic magnets, which currently represent by far the most powerful magnets. MA in metals has a very rich and complicated physics as a function of concentration and temperature (see, for instance, "magnetic chameleon" in Refs. [4,5]) which requires detailed knowledge of the electronic structure at and around the Fermi level. Theoretically, very extended studies of MA phenomena have been done based on the traditional k-space analysis [6,7]. For many theoretical models, however, a physical picture based on real-space decomposition of relativistic magnetic interactions can often be more useful. From the point of view of searching for new magnetic materials, the replacement of some atoms (chemical doping) is a very common procedure (see a recent review [8]). Due to all these factors, questions such as: "how long ranged are anisotropic interactions?," "when can we use a single-ion approximation?," and "what is the influence of hybridization on the spatial dependence of magnetic anisotropy?" require answers in specific materials, especially metals, where all electronic interactions are expected to be long ranged due to Fermi surface effects. Thus, it is needed to be able to decompose the observed relativistic properties in the crystals to intra- and interatomic contributions including possible multiatomic interactions.

Such decomposition to on-site and pairwise interactions can be done using spin-orbit (SO) coupling as a perturbation with a Green's function formalism [9,10]. However, such methods are difficult to implement in modern full potential electronic structure studies that are based mostly on the nonorthogonal basis set Hamiltonian constructions. This is unfortunate as the majority of high-anisotropy systems must have noncubic symmetry (mostly tetragonal or hexagonal) with clear importance of nonspherical terms in the potential. From a different perspective, the relativistic perturbation theory can be questionable in the materials where, for instance, crystal field effects are small relative to relativistic effects (rare-earth atoms). Also, the traditional replacement of the total energy (TE) by its one-electron contribution [9,10] is a very uncontrolled approximation and the opportunity to decompose the exact TE is really needed. Thus, a general method for the analysis of atomic and interatomic relativistic interactions in arbitrary systems in popular Hamiltonian-based band structure methods is highly desired.

This paper presents a simple technique to solve this problem: We propose to consider the speed of light (c) in the description of certain valence electronic states of atom in the crystal as a variable. We first consider the spin-polarized Dirac equation. Inside the atom our zero-order Hamiltonian includes the scalar potential $V(\mathbf{r})$ and the effective magnetic field $\mathbf{B}(\mathbf{r})$:

$$H = c\boldsymbol{\alpha}\cdot\mathbf{p} + (\beta - 1)mc^2 + V(\mathbf{r}) + \beta\boldsymbol{\sigma}\cdot\mathbf{B}(\mathbf{r}). \quad (1)$$

Here, c is the speed of light, $\boldsymbol{\alpha}$ and $\boldsymbol{\beta}$ are standard Dirac 4×4 matrices, and $\mathbf{p}$ is the momentum operator. The three Cartesian components of the vector $\boldsymbol{\sigma}$ are the Pauli 2×2 matrices, and m is the electron rest mass. In the atomic Rydberg units $m = 1/2$ and $c \approx 274$. Thus, formally one can vary the inverse of the speed of light from 0 (its value in the nonrelativistic limit) to $\approx 1/274$ on all atomic sites or some of them. For each particular c value, the TE of relativistic DFT can be obtained variationally without needing constraining fields. The resulting TE $E\{c_{i\alpha}\}$ would be a functional of site index i and electronic quantum number (if needed), so we assume that the relativistic TE can be presented as a functional of

*Current address: Amazon, Seattle, WA 98109, USA.
†antropov@ameslab.gov

all c_i:

$$E = E\{c_i\}. \tag{2}$$

Now we consider a variation of the TE δE by changing the speed of light c on a single atomic site 1 while solving the atomic Dirac equation. Let us first assume a nearly nonrelativistic case $[(1/c_1)^2 = \alpha_1 \ll 1]$. After solving the band problem the corresponding variation of the TE (2) can be presented as

$$\delta E = \alpha_1 N + \alpha_1^2 A + \cdots, \tag{3}$$

where the first term corresponds to the linear variation of the TE, the second one to quadratic, and so on. Here the A term represents the TE variation on site 1 (intra-atomic contribution) while the term with N corresponds to energy change due to interatomic coupling of atom 1 with its surrounding. In a case of simultaneous variation of c on two sites 1 and 2 the TE variation can be presented in a similar way as

$$\delta E = \alpha_1^2 A + \alpha_1\alpha_2 C + \alpha_2^2 B + \alpha_1 N + \alpha_2 M \cdots, \tag{4}$$

where A and B are pure intra-atomic parts, the C term corresponds to the interatomic interaction of atoms 1 and 2, and the $N(M)$ terms describe pairwise interatomic couplings of atom 1 (2) with all other atoms [except atom 2 (1)].

For the case of MA symmetric interactions, one can repeat describing the above action for different directions of the magnetization and for the MAE we will have similar decomposition,

$$K = \alpha_1 N + \alpha_1^2 A + \ldots, \tag{5}$$

with A corresponding to the single-site anisotropy contribution and N to the sum of pairwise MA terms. The expansion (5) already contains only small MA terms, while Eq. (3) describes much larger changes of relativistic TE (including, for instance, the variation of scalar relativistic terms such as Darwin and mass velocity in a case of perturbation theory usage).

The expansions above can also be illustrated using a perturbation theory approach if we use the atomic SO coupling as a smallness parameter. Then the analog of Eq. (4) for two sites i and j can be presented as

$$K = \lambda_i^2 A + 2\lambda_i\lambda_j C + \lambda_j^2 B, \tag{6}$$

where λ_i is a SO coupling parameter on site i. This simple example demonstrates a basic idea of this paper: decomposition of the total relativistic energy or its angular variation (anisotropic torque) to intra- and interatomic terms. Evidently, considering the full angular dependence of E in magnetic relativistic cases, one can obtain the desired spatial dependencies of the symmetric anisotropic energy terms. In a case of anisotropic magnetic interactions (such as Dzyaloshinskii-Moriya interaction), the speed of light change would affect the small angle between moments on different sites and directly provides an opportunity to estimate the strength of this interaction as well.

The main advantage of this scheme is an opportunity to obtain relativistic intersite interactions using highly precise electronic structure codes with no shape approximation for the potential. Second, this scheme can be used for the exact decomposition of the TE with or without any relativistic perturbation theory formalism. Naturally it can be used for any approximate description of the TE as well, including its one-electron contribution (see Refs. [9,10]) or just SO energy analysis (see below).

So far, we discussed a decomposition of the TE without any approximation. While there are no concerns about such calculations, in some cases one can use simplified methods to obtain the TE. For instance, there are many approximate ways of presenting the TE as a sum of the atomic contributions. As usual, such "quasiatomic" partial contributions represent a sum of pure atomic energy and interatomic contributions. One of the most popular techniques, for instance, is the replacement of the TE by the consideration of its one-electron contributions in DFT-based methods (see Refs. [11,12]).

While our proposed scheme is introduced for the fully relativistic spin-polarized approach [13], it is still more convenient to combine this proposal with a perturbative scheme to separate small anisotropic terms from large isotropic ones. A qualitative advantage of the relativistic perturbative theory is that the major relativistic interaction responsible for the magnetic anisotropy can be separated from all others in the second order over c^{-2} as the SO coupling. A variation of the speed of light described above, in turn, can be replaced by a variation of SO coupling alone. Earlier, we implemented a variation of SO coupling to study the applicability of relativistic perturbation theory and a relativistic virial theorem [14] without discussion of interatomic interactions. Similar studies with the removal SO coupling have been done in Ref. [15] to understand MAE for adatoms and monolayers.

Below we will concentrate on the analysis of MAE. The most valuable information we would like to obtain is the knowledge of the key contributor to the enhancement of MAE. As we will demonstrate below, this can be done by creating a site anisotropy diagram as a function of a particular atomic SO coupling (or any of its electronic orbital components). It can be obtained using a partial one-electron contribution analysis or by the calculation of atomic SO coupling energy (E_{so}) which is directly related to the total relativistic energy change when SO coupling is added [16]. We will be using these perturbation theory SO energy calculations due to the good accuracy of perturbation theory in d-metals. The analysis of one-electron contribution has been used since the 1960s [9,10] and represents a very uncontrolled approximation. The "local force theorem" [11,12] cannot be justified in this case, as it is formulated for variations only, while in the calculation of MAE one has to use the finite differences.

In this work, we first test our approach for the well-known magnet CoPt which can be considered as a prototype system with a nontrivial site decomposition of MAE. We then consider the more complicated magnet $Fe_{16}N_2$ doped by Bi, Sb, Co, and Pt atoms. Both structural stability and MAE will be studied. The reason to choose these dopants is that they have very different electronic structures: Pt has a localized d state, while Bi and Sb show a spreading delocalized p state. By decomposing the calculated MAE in terms of atomic SO coupling anisotropies, we show in detail how the SO coupling interaction of the dopants with different electronic structures affects the MAE of $Fe_{16}N_2$ compounds.

II. METHODS

First-principles calculations were carried out using the density functional theory (DFT) with spin polarization. The generalized gradient approximation (GGA) in the form of the PBE (Perdew, Burke, and Ernzerhof [17]) exchange correlation functional implemented in the VASP code [18] was used. Kinetic energy cutoff was set to 650 eV. The Monkhorst-Pack scheme [19] was used for Brillouin zone sampling with a k-point grid resolution of $2\pi \times 0.033$ Å^{-1} during the structure optimization. The ionic relaxation was stopped when the force on each atom became smaller than 0.01 eV/Å. The MAE calculations were also performed with the VASP code. All symmetry operations were switched off completely when the SO coupling was turned on. A denser k-point grid ($2\pi \times 0.016$ Å^{-1}) was used in the MAE calculations to achieve a better k-point convergence. To obtain the MAE, we first performed a fully self-consistent collinear calculation. Then we started from the charge density and performed one-shot calculations with SO coupling and different orientations of magnetization direction aligned along [001] and [100] to get the total energies $E^{[001]}$ and $E^{[100]}$, respectively [20]. The SO coupling can also be calculated with self-consistent calculation. The decomposition scheme works for both cases.

III. RESULTS AND DISCUSSION

We first consider a well-known CoPt ferromagnet. This layered tetragonal system (AuCu structural type) shows a very large MAE (comparable to those in rare-earth magnets) and has been studied many times in the past. All calculational parameters have been taken as in Ref. [14] with k-point mesh $24 \times 24 \times 26$. The unusual feature of this system is that the MAE in CoPt (as shown in [16]) does not follow the anisotropy of the orbital moment and cannot be described by Streever's model [9,21].

Our calculated total MAE is 0.84 meV and it agrees well with earlier full-potential results [14,16] and the experiment [22]. As we mentioned above, to obtain the desired spatial decomposition of this number, one can use the exact TE calculations as we suggested in the beginning and/or approximate methods such as one-electron and SO coupling energies calculated at each site. The latter two are closely related. Within the second-order perturbation theory, it has been shown [16] that the total MAE of a hexagonal or tetragonal crystal can be written as

$$K_{\mathrm{MAE}} = \sum_i K_{\mathrm{so}}(i)/2, \tag{7}$$

where $K_{\mathrm{so}}(i)$ is the anisotropy of SO coupling energy from the atom i and the summation includes all atoms in the unit cell. $K_{\mathrm{so}}(i) = E_{\mathrm{so}}^{[100]}(i) - E_{\mathrm{so}}^{[001]}(i)$, where $E_{\mathrm{so}}^{[001]}(i)$ and $E_{\mathrm{so}}^{[100]}(i)$ are SO coupling energies of the atom i with the magnetization aligned in the [001] and [100] directions, respectively.

For simplicity, we consider the same change for all atomic valence electrons, but any orbital decomposition can be done in the same way. Technically, we introduce an artificial modification of SO coupling strength on the doping site to investigate how $K_{\mathrm{so}}(i)$ on the other atoms changes by tuning the SO coupling strength on the dopant. Within the standard relativistic perturbation theory [23], the SO coupling Hamiltonian has the form

$$\hat{H}_{\mathrm{SOC}} = \xi \hat{\sigma} \cdot \hat{L}, \tag{8}$$

where $\hat{\sigma}$ is a Pauli spin operator, and $\hat{L}$ is the angular momentum operator. The SO coupling strength ξ is proportional to the radial derivative of the spherical part of the effective all-electron potential $V(r)$ within the augmentation atomic sphere as

$$\xi = \frac{\lambda}{c^2} \frac{\hbar^2}{r(2m_e)^2} \frac{dV(r)}{dr}. \tag{9}$$

Here we employ a scaling factor λ in Eq. (9) for any atom. We gradually vary λ from 0 to 1 and in this case perform *self-consistent* calculations with SO coupling [24] to obtain the corresponding TE and $K_{\mathrm{so}}(i)$ as the function of λ. In the case where one needs to extract any orbital-dependent decomposition, a scaling factor $\frac{\lambda}{c^2}$ in the SO Hamiltonian can be introduced just for a specific orbital.

Thus, we initially vary SO coupling on atoms inside a single-layer i in CoPt and calculate the resulting atomic MAE on each layer in our supercell. While the change of the $\mathrm{K_{so}}(i)$ on-site i will be a sum of the pure intra-atomic (proportional to λ_i^2) and many intersite terms ($\lambda_i \lambda_j$), the change $K_{\mathrm{so}}(i)$ on other atoms will be the result of the intersite interactions only. Thus, one can clearly extract all pairwise interactions just from a variation of SO coupling on a given site. Functional dependence on λ_i allows us to determine the effective spatial decomposition of anisotropy.

Our results indicate that the Pt atoms in CoPt produce the dominant part of the MAE (0.96 meV), while the Co subsystem has a small and negative (–0.085 meV) contribution to the total MAE. According to Eq. (1), these quantities in turn can be presented as a corresponding sum of the pure on-site ("single-ion") and all intersite terms. Using a variation of λ, we obtain the desired spatial decomposition. It appears that the pure on-site term dominates the Pt atom MAE (0.85 meV) while the total contribution from the first nearest neighbor (NN) Co atoms ($K_{\mathrm{Pt-Co}}$) is nearly—five to six times smaller and negative (–0.15 meV). Simultaneously, the total pairwise contribution from the NN Pt atoms along the z direction ($K_{\mathrm{Pt-Pt}}$) is positive and is the largest intersite interaction in the system (0.22 meV). Interlayer interactions beyond these two NN are smaller in amplitude and oscillating. The total MAE on the Co atom is small and negative due to the domination of negative pairwise contributions from Pt atoms (–0.15 meV). While the Co atom on-site anisotropy is positive it is too small to compete even with negative pairwise Pt-Co interactions. Thus, the Pt atom contributions are absolutely dominating, providing a strong and positive Pt on-site anisotropy, somewhat smaller positive Pt-Pt, and negative Pt-Co two-site anisotropies. These results are in qualitative agreement with those obtained a long time ago in Ref. [10] using the Green's function method and the atomic sphere approximation. Our results of anisotropy calculations using the TE and SO coupling analysis deviate from each other insignificantly (1%–4%).

Next, we switch to the magnet $Fe_{16}N_2$. The pure $Fe_{16}N_2$ phase (space group $I4/mmm$) contains three Wyckoff

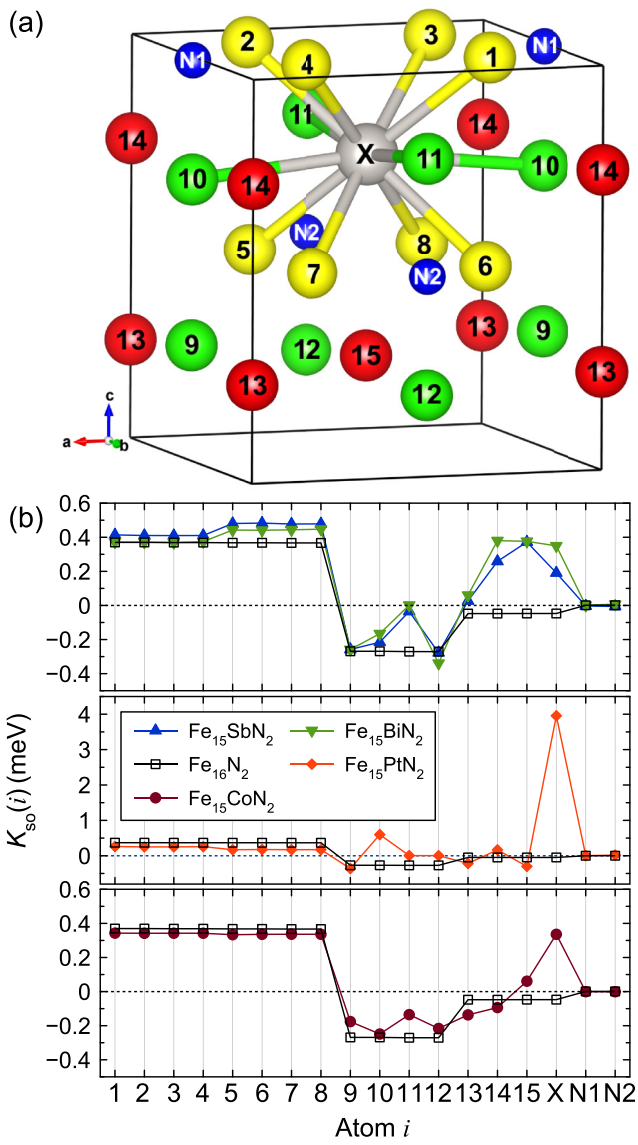

FIG. 1. (a) Crystal structure of $Fe_{16}N_2$ with doping X. Yellow are Fe 8h, red are Fe 4d, green are Fe 4h positions, and blue are N atoms. X is the dopant at the 4d site. (b) The SO coupling anisotropy K_{so} of each atom. Note the scale of the middle panel is different.

positions for Fe: 4d, 4e, and 8h. As shown in Fig. 1(a), we mainly consider the doping on the 4d position. The 4d position has eight Fe-8h sites as the first NNs and four Fe-4e sites as the second NNs.

To obtain a reasonable estimate of energy stability, all the crystal structures are first relaxed by the DFT. The obtained lattice parameters are shown in Table I. For pure $Fe_{16}N_2$, the volume from the DFT is slightly smaller than the room-temperature experimental data [25] ($a = 5.72$ Å, $c = 6.29$ Å). This is reasonable as the calculation is done at $T = 0$ K. Doping with Bi, Sb, and Pt atoms all expands the lattice. Doping with the Co atom keeps the lattice almost unchanged.

The energy stabilities are considered based on the formation energy (E_f) and the energy relative to the convex hull (E_c). Here we take $Fe_{15}SbN_2$ as an example to illustrate how the E_f and E_c are calculated. In this case, the formation energy is defined by

$$E_f(Fe_{15}SbN_2) = E(Fe_{15}SbN_2) - \tfrac{15}{18}E(Fe) - \tfrac{1}{18}E(Sb) - \tfrac{2}{18}E(N), \quad (10)$$

where $E(\cdot)$ is the TE (per atom) of the corresponding phase. In this case, the reference phases are the 0 K ground-state structures of elementary Fe ($bcc - Im\bar{3}m$), Sb ($R\bar{3}m$), and N ($Pa\bar{3}$), respectively. A *negative* formation energy indicates the compound is energetically favorable against phase decomposition. The energy relative to the convex hull E_c is relevant to the experimental synthesizability. The convex hull is composed of planes (curves if binary) connecting the formation energies of all thermodynamically stable phases. To compute the energy relative to the convex hull (E_c), one needs to consider the closest stable phases near the concertation, which can be found in the Materials Project database [26]. Here, for $Fe_{15}SbN_2$, the surrounding phases on the ternary phase diagram are Fe ($Im\bar{3}m$), Fe_3N ($P6_322$), and $FeSb_2$ ($Pnnm$). Therefore, E_c is calculated as

$$E_c(Fe_{15}SbN_2) = E(Fe_{15}SbN_2) - \tfrac{8.5}{18}E(Fe) - \tfrac{2}{18}E(Fe_3N) - \tfrac{0.5}{18}E(FeSb_2). \quad (11)$$

When $E_c = 0$, the compound is thermodynamically stable. A compound with a smaller E_c indicates a higher possibility to be synthesized in experiments. As a reference, it was found that 80% of compounds in the Inorganic Crystal Structure Database [27] have an E_c of less than 36 meV per atom [28].

Examining the energy values in Table I, one can see that pure $Fe_{16}N_2$ has a very small E_c. This is consistent with the fact that it can be synthesized by the experiment. It is also interesting to note that the compounds Sb, Pt, and Co also have small values for E_c (in a range of 20–30 meV/atom). This suggests that it is possible to form these compounds through experimental synthesis [28]. In contrast, the Bi-doped $Fe_{16}N_2$ has positive formation energy and it is thermodynamically unstable against phase separation. Therefore, except for the

TABLE I. Optimized lattice parameters (a, c), the formation energy (E_f), the energy above the convex hull (E_c), and its reference.

Compounds	a (Å)	c (Å)	E_f (meV/atom)	E_c (meV/atom)	Reference phases in E_c calculations
$Fe_{16}N_2$	5.68	6.22	–33.3	4.5	Fe, Fe_3N
$Fe_{15}BiN_2$	5.76	6.34	63.2	–	Fe, Bi, N
$Fe_{15}SbN_2$	5.72	6.30	–8.8	31.0	Fe, Fe_3N, $FeSb_2$
$Fe_{15}PtN_2$	5.72	6.27	–38.5	32.8	Fe, Fe_3N, Fe_3PtN
$Fe_{15}CoN_2$	5.68	6.21	–27.8	20.7	Fe, Fe_3N, Fe_3Co

TABLE II. Magnetic anisotropy energy K_{MAE}, magnetocrystalline anisotropy constant (K_1), half of the total SO coupling anisotropy ($\sum K_{\mathrm{SO}}/2$) and the difference between K_{MAE} and $\sum K_{\mathrm{SO}}/2$.

Compounds	K_{MAE} (meV/cell)	K_1 (MJ/m^3)	$\sum K_{\mathrm{SO}}/2$ (meV/cell)	$\Delta = \frac{\lvert K_{\mathrm{MAE}} - \sum K_{\mathrm{SO}}/2 \rvert}{K_{\mathrm{MAE}}}$
$Fe_{16}N_2$	0.846	0.682	0.840	0.70%
$Fe_{15}BiN_2$	1.854	1.415	1.838	0.86%
$Fe_{15}SbN_2$	1.796	1.395	1.808	0.67%
$Fe_{15}PtN_2$	3.348	2.613	2.794	17%
$Fe_{15}CoN_2$	1.044	0.835	1.049	0.48%

Bi-doped $Fe_{16}N_2$, other doped compounds considered in this work would be achieved by experiments.

We now consider the effect of doping on the MAE in $Fe_{16}N_2$. Table II shows the MAE for the relaxed structures computed by the VASP code [18] as described in the method section (denoted as K_{MAE} with the unit of meV/cell and K_1 with the unit of MJ/m^3, respectively). Based on our calculations, the value of K_1 in pure $Fe_{16}N_2$ is 0.682 MJ/m^3. This is consistent with experimental reports in a range of 0.44–2.0 MJ/m^3 [29–33] as well as previous DFT calculations [34–36]. Our calculations show that the MAE is improved by all considered dopants: Compared to $Fe_{16}N_2$, Bi and Sb dopants increase the anisotropy by a factor of 2, and Pt doping increases the MAE more than four times. Co doping provides a slight increase in MAE.

Next, we proceed with the decomposition of the total MAE into the contributions from different atomic sites to explore the spatial distribution of this MAE enhancement. In Table II, we examine the validity of Eq. (7) in the current systems. It shows the relation is very valid for $Fe_{16}N_2$, $Fe_{15}BiN_2$, $Fe_{15}SbN_2$, and $Fe_{15}CoN_2$ (the deviations are all within 1%). For $Fe_{15}PtN_2$, the discrepancy is much larger (17%), indicating possible importance of higher–order terms of perturbation theory.

In Fig. 1(b), the SO coupling anisotropy energies of each atomic site [$K_{\mathrm{so}}(i)$] in $Fe_{16}N_2$ and the four doped compounds are plotted. In pure $Fe_{16}N_2$, K_{so} of the 8*h* sites [sites Fe1–Fe8 in Fig. 1(a)] promotes the MA along the easy axis (001) while 4*h* sites K_{so}(Fe9–Fe12) prefer an in-plane direction. K_{so} at the 4*d* sites (Fe13–Fe15 and *X*) overall are not significant. For the doped structure, the atoms are reindexed because the symmetry of the original Wyckoff positions is broken. Compared to $Fe_{16}N_2$, the K_{so} for most Fe atoms in the unit cell is larger and positive upon Sb and Bi doping. The most significant increases of K_{so} caused by Bi and Sb are at the sites Fe14 and Fe15. They are both initially 4*d* sites, and neither is the first NNs (Fe1–Fe8) or second NNs (Fe10 and Fe11) of the doped site. Therefore, the effect of doping on K_{so} is not very short ranged but goes well beyond the nearest atomic shells of the dopants. The mechanism of change in K_{so} due to Pt doping is different from Sb and Bi doping. Pt induced a strong K_{so} by itself. While it slightly hindered the anisotropy along the [001] direction at 8*h* Fe13 and Fe15 sites, the magnitude K_{so} of Pt is so huge that the overall MAE is still significantly enhanced.

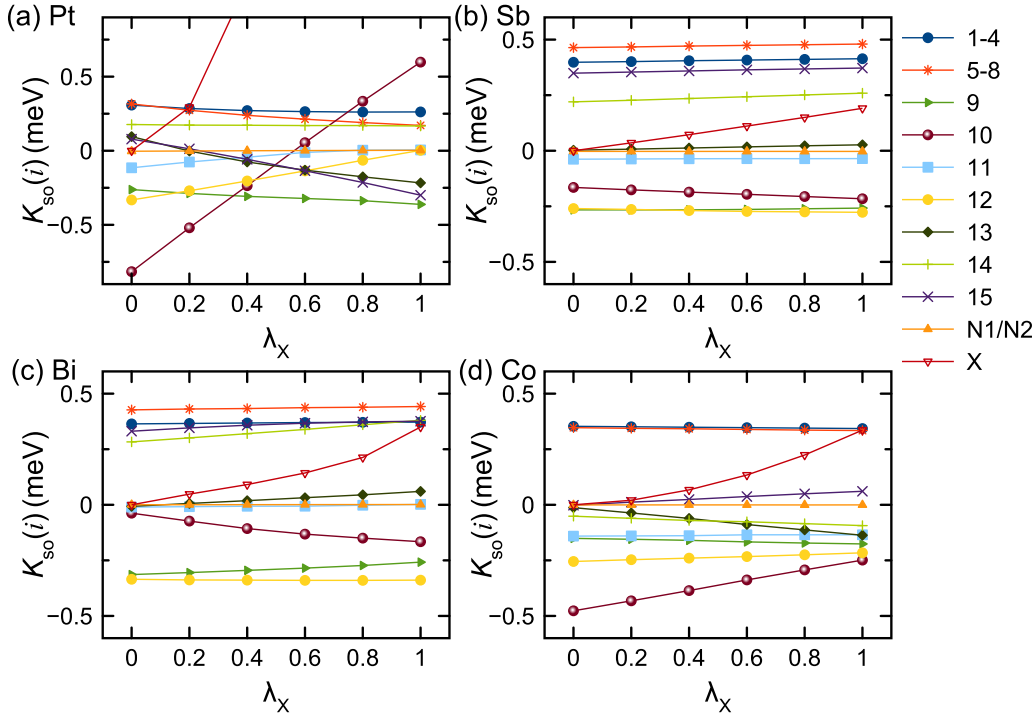

FIG. 2. The atomic SO coupling anisotropy energy $K_{\mathrm{so}}(i)$ as a function of the scaling factor λ on the doping site (Fe16) for the four doped structures. For each curve all the λ are fixed except the λ_X varies. Only 1, 5, and N1 are shown because 1–4, 5–8, N1/N2 sites are equivalent.

Co doping increased part of K_{so} along the easy axis ($4h$ sites) but also increased the anisotropy of atoms along the hard axis ($8d$ sites). This cancellation results in a very slight change of MAE from its pure $Fe_{16}N_2$ value.

To decompose the atomic magnetic anisotropies, we proceed with an adjustment of the speed of light (or SO coupling of the valence electrons on a particular atomic site) described above. Figure 2 plots K_{so} on all sites in our supercell as a function of SO strength λ_X on the doping site X. It shows that a change of K_{so} on all other atoms is a linear function of λ_X because this change is induced by a pairwise interaction. In turn, dopant K_{so} changed as λ_X^2 and clearly demonstrated a quadratic behavior in Fig. 2. The K_{so} of the Pt dopant is large (around 4 meV at $\lambda_X = 1$) and is not shown in Fig. 2(a). In all cases, the Fe10 site shows the strongest interaction with the dopant ($K_{X-\mathrm{Fe10}}$ interaction) as its anisotropy K_{so} always changed most significantly with λ_X. In the case of Pt, the slope of anisotropy dependence on the Fe12 site is also correlated with the slope of K_{so} on the Pt site (positive pairwise interaction). For other dopants, the anisotropies of majority atoms were almost independent of λ_X. This supported the somewhat "single-ion" character of dopant MA. On the other hand, different Fe sites exhibited weak but different sign changes of K_{so} as λ_X changed from 0 to 1. This indicated different signs of pairwise interactions with this particular Fe dopant. Figure 2 clearly shows that in many cases the pairwise interactions strongly influence some atomic anisotropies, changing both their amplitudes and signs. The first, second, and even third NNs anisotropic interactions $K_{\mathrm{Pt-Fe}}$ can be larger than pure single-site contribution K_{Fe}. Overall, the MAE is not limited by intra-atomic and NN couplings; more distant neighbors should be included into consideration. Clearly—three to five shells of neighboring atoms have to be considered. Such itinerant effects would strongly affect the temperature dependence of magnetic anisotropy in these systems. We also note that the difference between the results for $\lambda = 0$ and $\lambda = 1$ in pure $Fe_{16}N_2$ and in the doped systems allows us to separate the effects of chemical bonding (hybridization) contributions to the intersite anisotropies through doping from changes created by SO coupling of the dopant. For example, the hybridization effect can be seen from the nonslope curves of atoms 11, 14, and 15 in the case of Sb and Bi doping, while the strong effect of SO coupling on atom 10 in Pt doping can be clearly identified from the large slope in Fig. 2.

IV. CONCLUSION

We proposed a method of decomposition of the total relativistic energy in solids to intra- and interatomic orbital contributions. The technique is based on a site/orbital variation of the speed of light in a particular term of relativistic electronic Hamiltonian (in our case the spin-orbit coupling). It does not require the use of traditional Green's function methods and naturally allowed us to study the spatial decomposition of the total energy in precise modern band structure methods without any approximations for the shape of the potential. It also does not require any approximate treatment of the total energy including very popular analysis of its one-electron component. This technique can be used when other relativistic interactions, such as dipole-dipole or spin-other-orbit are considered. As an illustration of the method, we tested such decomposition in the case of the magnet CoPt, and then we analyzed the pairwise interactions in α''-$Fe_{16}N_2$ doped by Bi, Sb, Co, and Pt on the $4d$ site. The site decomposition revealed the most important pairwise interactions and showed different mechanisms of increasing magnetocrystalline anisotropy for the Pt and Bi/Sb dopants. We found that the anisotropic interactions in studied metallic systems are relatively long ranged with pairwise contributions often being larger than on-site ones. Theoretically considered dopants increased the magnetocrystalline anisotropy of the original $Fe_{16}N_2$ phase. Our studies of structural properties of these alloys predicted the possible stability of some doped systems. This created an opportunity for the experimental verification of our predictions.

ACKNOWLEDGMENTS

The majority of this work was done at Ames Laboratory and is supported by the US Department of Energy (DOE), Office of Science, Basic Energy Sciences, Division of Materials Science and Engineering, including the computer time support from the National Energy Research Scientific Computing Center (NERSC) in Berkeley, CA. Ames Laboratory is operated for the DOE by Iowa State University under Contract No. DE-AC02-07CH11358. M.C.N. also acknowledges the partial support from the National Science Foundation (NSF) Award No. DMR-1729677. Y.S. was partially supported by NSF Awards No. EAR-1918134 and No. EAR-1918126.

[1] E. R. Callen and H. B. Callen, J. Phys. Chem. Solids **16**, 310 (1960).
[2] N. Akulov, Z. Phys. **100**, 197 (1936).
[3] H. B. Callen and E. Callen, J. Phys. Chem. Solids **27**, 1271 (1966).
[4] A. Iga, Jpn. J. Appl. Phys. **9**, 415 (1970).
[5] I. A. Zhuravlev, V. P. Antropov, and K. D. Belashchenko, Phys. Rev. Lett. **115**, 217201 (2015).
[6] E. I. Kondorskii and E. Straube, Zh. Eksp. Teor. Fiz. **63**, 356 (1972) [Sov. Phys. JETP **36**, 188 (1973)].
[7] E. I. Kondorskii and E. Straub, Pis'ma Zh. Eksp. Teor. Fiz. **17**, 41 (1973) [JETP Lett. **17**, 29 (1973)].
[8] V. N. Antonov and V. P. Antropov, Low Temp. Phys. **46**, 1 (2020).
[9] K. Yosida, A. Okiji, and S. Chikazumi, Prog. Theor. Phys. **33**, 559 (1965).
[10] I. V. Solovyev, P. H. Dederichs, and I. Mertig, Phys. Rev. B **52**, 13419 (1995).
[11] A. K. Mackintosh and O. K. Anderson, in *Electrons at the Fermi Surface*, edited by M. Springford (Cambridge University Press, Cambridge, 1975).
[12] V. Heine, in *Solid State Physics*, edited by H. Ehrenreich, F. Seitz, and D. Turnbull (Academic Press, New York, 1980).

[13] I. V. Solovyev, A. I. Liechtenstein, V. A. Gubanov, V. P. Antropov, and O. K. Andersen, Phys. Rev. B **43**, 14414 (1991).
[14] M. C. Nguyen, Y. Yao, C.-Z. Wang, K.-M. Ho, and V. P. Antropov, J. Phys.: Condens. Matter **30**, 195801 (2018).
[15] O. Šipr, S. Bornemann, H. Ebert, and J. Minár, J. Phys.: Condens. Matter **26**, 196002 (2014).
[16] V. Antropov, L. Ke, and D. Åberg, Solid State Commun. **194**, 35 (2014).
[17] J. P. Perdew, K. Burke, and M. Ernzerhof, Phys. Rev. Lett. **77**, 3865 (1996).
[18] G. Kresse and J. Furthmüller, Comput. Mater. Sci. **6**, 15 (1996).
[19] H. J. Monkhorst and J. D. Pack, Phys. Rev. B **13**, 5188 (1976).
[20] S. Steiner, S. Khmelevskyi, M. Marsmann, and G. Kresse, Phys. Rev. B **93**, 224425 (2016).
[21] R. L. Streever, Phys. Rev. B **19**, 2704 (1979).
[22] A. Y. Yermakov and V. V. Maykov, Phys. Met. Metallogr. **69**, 198 (1990).
[23] L. D. Landau and E. M. Lifshitz, *Quantum Mechanics: Non-relativistic Theory* (Pergamon Press, Oxford, 1977), Vol. 3.
[24] P. Blaha, K. Schwarz, G. K. H. Madsen, D. Kvasnicka, J. Luitz, R. Laskowski, F. Tran, and L. D. Marks, *WIEN2K, An Augmented Plane Wave + Local Orbitals Program for Calculating Crystal Properties* (Technische Universität Wien, 2018).
[25] K. H. Jack, Proc. R. Soc. London, Ser. A **208**, 200 (1951).
[26] A. Jain, S. P. Ong, G. Hautier, W. Chen, W. D. Richards, S. Dacek, S. Cholia, D. Gunter, D. Skinner, G. Ceder, and K. A. Persson, APL Mater. **1**, 011002 (2013).
[27] M. Hellenbrandt, Crystallogr. Rev. **10**, 17 (2004).
[28] Y. Wu, P. Lazic, G. Hautier, K. Persson, and G. Ceder, Energy Environ. Sci. **6**, 157 (2013).
[29] Y. Sugita, K. Mitsuoka, M. Komuro, H. Hoshiya, Y. Kozono, and M. Hanazono, J. Appl. Phys. **70**, 5977 (1991).
[30] H. Takahashi, M. Igarashi, A. Kaneko, H. Miyajima, and Y. Sugita, IEEE Trans. Magn. **35**, 2982 (1999).
[31] S. Uchida, T. Kawakatsu, A. Sekine, and T. Ukai, J. Magn. Magn. Mater. **310**, 1796 (2007).
[32] E. Kita, K. Shibata, H. Yanagihara, Y. Sasaki, and M. Kishimoto, J. Magn. Magn. Mater. **310**, 2411 (2007).
[33] N. Ji, M. S. Osofsky, V. Lauter, L. F. Allard, X. Li, K. L. Jensen, H. Ambaye, E. Lara-Curzio, and J. P. Wang, Phys. Rev. B **84**, 245310 (2011).
[34] X. Zhao, C. Z. Wang, Y. Yao, and K. M. Ho, Phys. Rev. B **94**, 224424 (2016).
[35] L. Ke, K. D. Belashchenko, M. van Schilfgaarde, T. Kotani, and V. P. Antropov, Phys. Rev. B **88**, 024404 (2013).
[36] I. Khan and J. Hong, Curr. Appl. Phys. **18**, 526 (2018).